Food Research International 219 (2025) 116976

Contents lists available at ScienceDirect

Food Research International

journal homepage: www.elsevier.com/locate/foodres

Protective effect of osmanthus water extract on liver dysfunction caused by DBP based on organoids and organ chips technologies

Qing Feng [a,i,1], Hongguo Chen [b,1], Meng Ren [a], Yongkang Qiao [c], Jingjing Zou [b], Xiao Liang [a], Ling Yu [d], Yang Wu [e,f], Shaohui Chen [a], Yanling Sun [a], Cuiyu Bao [a], Xu Yang [a,g,h], Ping Ma [a,g,*], Surui Lu [a,**]

[a] Key Laboratory of Environmental Related Diseases and One Health, Xianning Medical College, Hubei University of Science and Technology, Xianning 437100, China
[b] National Forestry and Grassland Administration Engineering Research Center for Osmanthus fragrans, Hubei University of Science and Technology, Xianning 437100, China
[c] Centre for Biological Science and Technology, Key Laboratory of Cell Proliferation and Regulation Biology of Ministry of Education, Faculty of Arts and Sciences, Beijing Normal University, Zhuhai 519000, China
[d] Southwest University, School of Materials and Energy, Chongqing 400715, China
[e] China National Biotec Group Adnova Co. Ltd., Wuhan 430073, China
[f] State Key Laboratory of Novel Vaccines for Emerging Infectious Diseases, Beijing 100098, China
[g] Hubei Industrial Technology Research Institute of Intelligent Health, Xianning 437100, China
[h] Institute of Eastern-Himalaya Biodiversity Research, Dali University, Dali 671003, Yunnan, China
[i] Hubei Key Laboratory of Diabetes and Angiopathy, School of Pharmacy, Xinning Medical College, Hubei University of Science & Technology, Xianning 437100, PR China

ARTICLE INFO

Keywords:
Osmanthus water extract
Dibutyl phthalate
Organoids
Organ chips
Metabolomics analysis

ABSTRACT

This study aimed to investigate the protective mechanism of *Osmanthus fragrans* water extract (OSF) against liver injury induced by dibutyl phthalate (DBP). We utilized liver organoids and liver organ chip technology to replicate the liver microenvironment in vivo. Metabolomic analysis revealed that DBP induced oxidative stress and lipid metabolism disorders; however, following intervention with OSF, the associated abnormal metabolites were significantly reduced. Molecular docking studies demonstrated the binding of its active ingredients to key targets. The primary findings indicate that OSF can effectively mitigate liver damage caused by DBP. This extract is anticipated to serve as a potential natural therapeutic agent for the prevention and treatment of DBP-induced liver dysfunction, thereby providing a theoretical foundation for future research and development.

1. Introduction

Recently, there has been a significant increase in interest regarding the study of bioactive metabolites found in plant-derived foods. These compounds are essential in addressing the pathological mechanisms associated with various human diseases, such as cancer, microbial infections, cardiovascular disorders, and metabolic disturbances. Plant-sourced foods serve as rich reservoirs of secondary metabolites, which exhibit diverse properties and hold considerable potential in the medical field. These plants contain a variety of natural compounds that can effectively combat ROS (Huang et al., 2023). *Osmanthus fragrans*, commonly cultivated in China, has been referenced in ancient pharmacopoeias (Zhang et al., 2022). In the Ming Dynasty, Li Shizhen conducted a comprehensive exploration of the medicinal properties of *Osmanthus fragrans* in his highly influential work, "Compendium of Materia Medica." In traditional Chinese medicine, this plant is classified as a warm-natured and non-toxic herbal remedy. Research has indicated that the primary components of *Osmanthus fragrans* are terpenoids and flavonoids, which exhibit a diverse range of functions, including anti-cancer, antioxidant, anti-inflammatory, analgesic, and cardiovascular-protective effects (Zheng et al., 2017). Recently, metabolomics has emerged as a prominent technique for conducting in-depth research on medicinal plants. Metabolomic studies have demonstrated that the roots, stems, leaves, flowers, and fruits of *Osmanthus fragrans* all possess

* Corresponding author at: Hubei University of Science and Technology, No. 88 Xianning Avenue, Xianning 437100, China.
** Corresponding author.
E-mail addresses: maping@hbust.edu.cn (P. Ma), 20231017@hbust.edu.cn (S. Lu).
[1] Co-first authors: These authors contributed equally to this work.

https://doi.org/10.1016/j.foodres.2025.116976
Received 11 April 2025; Received in revised form 26 June 2025; Accepted 29 June 2025
Available online 1 July 2025

medicinal properties (Fu et al., 2022). Currently, *Osmanthus fragrans* is utilized in traditional Chinese medicine for the treatment of pain, cough, stomachache, diarrhea, and hepatitis (Luo et al., 2024).

Liver disease is becoming increasingly prevalent, affecting over 1.5 billion individuals in 2017, with more than half of these cases could be traced back to non-alcoholic fatty liver disease (NAFLD) (Kanabekova et al., 2022). This condition is responsible for more than 2 million deaths globally each year (Panwar et al., 2021). To investigate the mechanisms and treatments of liver disease, researchers have developed both animal models and two-dimensional (2D) cell models (Pingitore et al., 2019). However, each of these models has distinct limitations: 2D cell models are susceptible to variability, which can lead to inaccurate results (Yang et al., 2023), while animal models present challenges in their applicability to human biology due to interspecies differences. The benefits of three-dimensional (3D) multicellular spheroid cultures and organoids are becoming increasingly recognized (Panwar et al., 2021). Research on organoids dates back to 1907, and they have the capability to accurately replicate the characteristics of human tissues (Ahammed & Kalangi, 2024). Liver organoids can be obtained from a diverse range of sources (Brooks et al., 2021) and exhibit significant potential for disease modeling (Panwar et al., 2021) as well as drug efficacy evaluation (Brooks et al., 2021). Furthermore, the integration of microfluidic technology opens new avenues for research methodologies (Septiana et al., 2023).

In recent years, microfluidic chips have gained increasing traction as in vitro cell culture platforms (Sun et al., 2016). The organ chips concept, introduced in 2010, has become a focal point of research. This technology offers significant advantages, including miniaturization, high integration, and cost-effectiveness. It enables precise regulation of cells, eliminates the necessity for animal models, and facilitates real-time monitoring of tissues alongside personalized evaluations of drug efficacy (Wang et al., 2023). Over the past decade, it has rapidly evolved and garnered considerable attention across various aspects of disease research (Farooqi et al., 2021). As a crucial organ for detoxification, the liver has inspired the development of diverse chip models (Ribeiro et al., 2019). In comparison to traditional animal models, the three-dimensional microphysiological system of the liver chip can comprehensively represent the physiological and pathological characteristics of the liver, thereby enhancing the predictability of research outcomes (Moradi et al., 2020). 2D cell cultures often fail to accurately replicate human physiology, and animal models are limited by interspecies differences (Deng et al., 2023). Organ chips can circumvent the challenges associated with animal research (Mastrangeli & van den Eijnden-van Raaij, 2021) and effectively simulate key functions while creating an in vivo microenvironment (Sun et al., 2016). In the realms of liver disease modeling and drug testing, it has provided significant impetus for related scientific investigations (Farooqi et al., 2021).

Sufficient evidence indicates that exposure to DBP can readily induce oxidative stress and inflict damage on the liver, consequently leading to the development of liver disease (El-Kenawi & Ruffell, 2017). As a crucial molecule in cellular oxygen metabolism, reactive oxygen species (ROS) are beneficial in moderate amounts; however, excessive levels can be detrimental (Murphy, 2009). ROS not only causes tissue damage but also activates various signaling pathways (Cheng et al., 2019), triggers inflammation, respiratory chain failure, and DNA mutations, thereby interfering with cancer progression (Murthy & Narsaiah, 2021). An excess of ROS in hepatocytes can damage proteins, lipids, and DNA, compromising the structure and function of the liver (Murphy, 2009).

Exposure to DBP can induce disorders in lipid metabolism. Lipid hydroperoxides contribute to oxidative damage in the liver, which leads to dysfunction of membrane receptors and ultimately results in the formation of malondialdehyde (Murphy, 2009). The liver plays a vital role in metabolizing free radical compounds. When the concentration of free radicals surpasses that of antioxidants, homeostasis is disrupted, leading to lipid metabolism disorders (Banerjee et al., 2023). The liver is essential for the regulation of systemic lipid metabolism, and its dysregulation is linked to various diseases (Wu et al., 2021). Phthalates are known endocrine disruptors, and studies in animals have demonstrated that exposure to these compounds can alter lipogenesis and metabolism (Huang, Cheng, et al., 2022).

Metabolomics is a high-throughput analytical technology that employs liquid chromatography-mass spectrometry or nuclear magnetic resonance for the qualitative and quantitative analysis of small molecule metabolites in biological samples. This field emerged in the late 1990s (Zhu et al., 2021). As a significant branch of systems biology, it offers a comprehensive mapping of small molecules involved in cellular metabolism (Liu & Locasale, 2017), thereby elucidating the human body's response to various stressors. The biological responses identified through this field are widely utilized in diagnosing various diseases and serve as a powerful tool for identifying biomarkers (Miao et al., 2022). Given the complexity of liver metabolism, metabolomics is frequently employed in hepatotoxicity studies (Long et al., 2021), aiding in the identification of early biomarkers and metabolic pathways (Zhu et al., 2021). Furthermore, it provides insights into chemical risks across multiple domains, enhancing our understanding of overall system metabolism (Hernández-Mesa et al., 2021).

The research ideas of this article: This study explores the biochemical interactions and metabolic effects of OSF in a liver tissue model constructed using organoids and organ-on-a-chip technology. By exposing the model to DBP and OSF, we aim to investigate their impact on oxidative stress markers and lipid metabolism-related biochemical pathways. Through metabolomic analysis, we will systematically identify and compare metabolic alterations, providing insights into the chemical and biochemical mechanisms underlying OSF's role in metabolic regulation. This research seeks to elucidate the compositional and functional properties of OSF as a bioactive food component and its potential influence on oxidative balance and lipid metabolism in food-related applications.

Based on the results of previous studies and the current investigation, we propose the following scientific hypothesis: OSF can antagonize the hepatotoxicity induced by DBP, as illustrated in Fig. 1. The primary molecular mechanisms involved are as follows: 1) OSF has the capability to reduce ROS generated by DBP; 2) it upregulates the Nrf2 signaling pathway, promotes the production of antioxidant enzymes, and enhances cellular function; 3) it downregulates the NFκB signaling pathway, thereby reducing the inflammatory response; and 4) it upregulates the PPAR-α signaling pathway, alleviating lipid metabolism disorders and consequently diminishing liver damage induced by DBP. Based on these molecular mechanisms, exposure to the aqueous extract of *Osmanthus fragrans* appears to be effective in treating DBP-induced liver oxidative damage and lipid metabolism disorders.

2. Methods

2.1. Grouping and experimental treatments of this study

According to the experimental objectives and the results of the CCK8 assay, a total of 10 groups were established (see Table 1). Among these, the DBP 50 μM group was utilized to construct a liver injury model, selecting a concentration that both induces injury and maintains cell viability based on CCK8 results. The DBP + OSF protection group employed a 10-fold logarithmic gradient concentration (referencing Huang, Zhao, et al., 2022) to investigate the dose-effect relationship of OSF. The DBP + VitC group acted as a positive control to assess the model's sensitivity and the protective efficacy of OSF. The t-BHP group was implemented to establish an oxidative injury model, allowing for the isolation and validation of the antioxidant mechanism of OSF, thereby enhancing the rigor of conclusions through comparisons across injury models. The t-BHP + OSF 200 μM and t-BHP + VitC groups were designed to compare protective effects under different injury mechanisms and to validate the role of OSF against the efficacy of VitC. The single VitC group served as a positive control for oxidative protection.

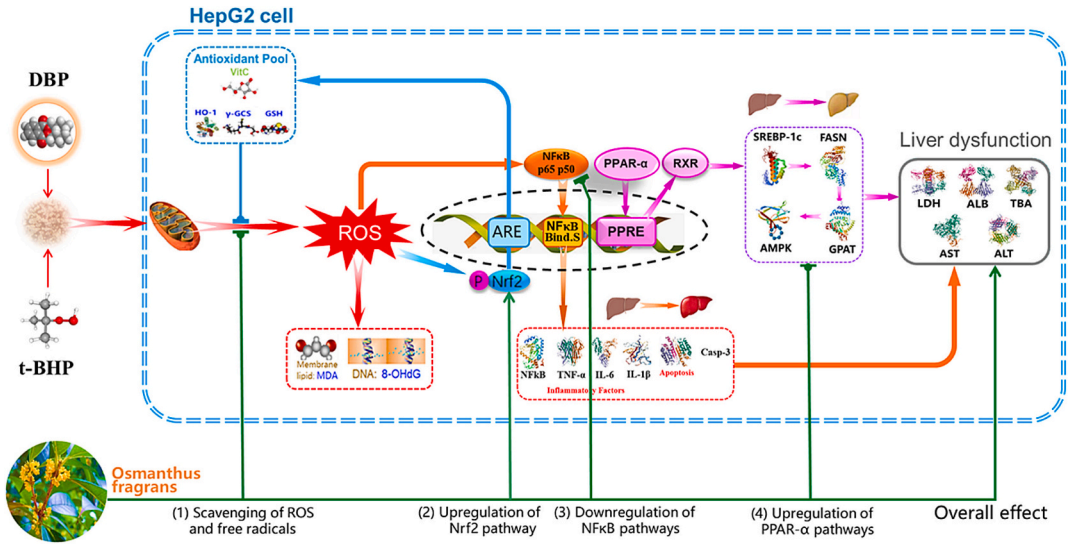

Fig. 1. Scientific hypothesis: the protective mechanism of OSF against the hepatotoxicity caused by DBP.

Table 1
Grouping and experimental treatments.

Group ID	Group names	Treatments for different groups					
		Treatment DBP 50 μM	Treatment OSF2 μM	Treatment OSF 20 μM	Treatment OSF 200 μM	Treatment t-BHP	Treatment VitC
Group1	Control	−	−	−	−	−	−
Group2	DBP 50 μM	+	−	−	−	−	−
Group3	DBP 50 μM + OSF 2 μM	+	+	−	−	−	−
Group4	DBP 50 μM + OSF 20 μM	+	−	+	−	−	−
Group5	DBP 50 μM + OSF 200 μM	+	−	−	+	−	−
Group6	DBP 50 μM + VitC	+	−	−	−	−	+
Group7	t-BHP	−	−	−	−	+	−
Group8	t-BHP + OSF 200 μM	−	−	−	+	+	−
Group9	t-BHP + VitC	−	−	−	−	+	+
Group10	VitC	−	−	−	−	−	+

2.2. Construction of a 3D polyglobule model of HepG2

As illustrated in Fig. 2A, HepG2 cells, which were cultured to the sixth passage, were counted and evenly distributed into an ultra-low adsorption U-shaped 96-well spherical culture plate. A total of 200 μL of cell suspension was added to each well. These cells were then cultured

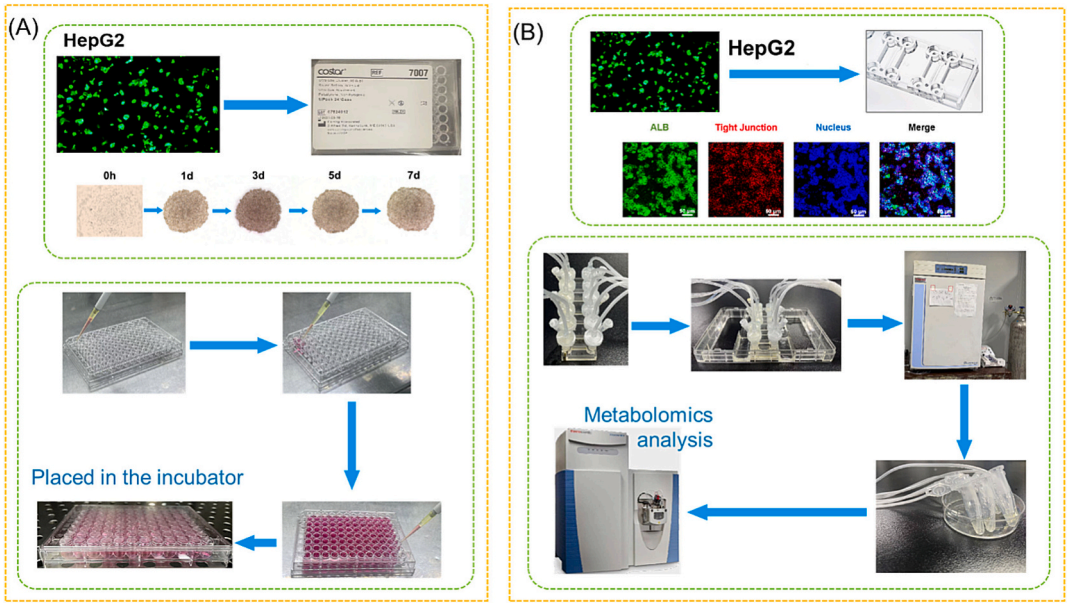

Fig. 2. Construction of liver organoids and liver organ chips. (A) Construction of liver organoids; (B) Construction of liver organ chips.

in a cell culture incubator at 37 °C with 5 % CO_2, leveraging the self-assembly properties of liver cells that enable them to spontaneously aggregate into spherical structures. Throughout the culture process, the polyspheres were replaced every two days, ensuring that the supernatant was carefully aspirated to avoid disturbing the polyspheres.

2.3. Construction of liver organ chips model

As illustrated in Fig. 2B, the experiment utilized GFP-labeled HepG2 cells that were cultured to the sixth passage. The microfluidic chip features a central channel with a width of 1.3 mm, flanked by lateral media channels on either side, each measuring 0.5 mm in width. The central channel is filled with fibrin hydrogel, which promotes the 3D growth of the cells. A microsyringe pump is connected to a sterile micropump extension tube to replenish the media channel on one side at a flow rate of approximately 10 μL/h. As demonstrated in Fig. S3, this arrangement allows DMEM medium to permeate into the central channel, thereby supporting cell growth. The cell growth process was monitored, as shown in Video 1 (\Video1.mp4) by seeding the cells and employing a miniature live cell monitoring system. The microfluidic chip contains a central region of fibronectin hydrogel designed to simulate liver tissue with cells, while two lateral channels facilitate the delivery of DMEM media. To prepare the mixture, 99 μL of cells (10^6 cells/mL) was dissolved in prewarmed DPBS, along with 20 μL of 15 mg/mL fibrinogen and 1 μL of 100 U/mL thrombin. This mixture was subsequently introduced into the central channel of the microfluidic chip and incubated for 40 min to promote gelation. Following gelation, the culture medium was introduced into two containers located above the same side through a sterile micropump extension tube, while another sterile micropump extension tube (without DMEM medium) was connected to collect the effluent. The chip was then incubated at 37 °Cwith 5 % CO_2 for 4 days. As shown in Fig. S4, after this incubation period, each exposure solution was added to the microfluidic chip and incubated for an additional 24 h at 37 °C with 5 % CO_2.

2.4. Detection of biomarkers in liver organoids

According to the previous CCK-8 and live and dead cell staining results (Figs. S1 and S2), various concentrations of exposure solutions (OSF, DBP, t-BHP, VitC) were added to the center of ultra-low adsorption U-shaped 96-well spherical culture plates. DBP was dissolved in DMEM at a concentration of 50 μM. Solutions of DMEM-DBP + OSF, DMEM-t-BHP, DMEM-t-BHP + OSF, and DMEM-VitC were prepared simultaneously and incubated at 37 °C in a 5 % CO_2 atmosphere. After incubation, the samples were washed three times with PBS, and the initial culture supernatant was collected. The contents were then detected according to the operating procedures and specifications outlined in the kit, measuring 8-OHdG, γ-GCS, HO-1, TNF-α, IL-6, IL-1β, Casp-3, NF-κB, Nrf-2, ALB, PPAR-α, RXR, SREBP-1c, FASN, GPAT, AMPK, GSH, LDH, and TBA. Additionally, the 3D spheres from each well in the different groups were extracted, washed three times with an appropriate amount of PBS buffer, and subsequently disrupted using a cell ultrasonic grinder on ice. After centrifugation at 4 °C at 12,000 rpm for 10 min, the supernatant was transferred to a 1.5 mL centrifuge tube for the detection of ROS, MDA, ALT, AST, T-CHO, and TG.

2.5. Immunofluorescence staining of zonula occludens-1 (ZO-1) and albumin (ALB)

ZO-1 is a crucial component of tight junctions between cells. Immunofluorescence staining of ALB reveals that albumin synthesis primarily occurs in the liver, which serves as its main production site. Liver diseases can impair hepatocytes, resulting in a diminished capacity to produce albumin and consequently a decrease in albumin levels. For a detailed description of the immunofluorescence staining method utilized in the liver organ chips, please refer to the Supplementary materials.

2.6. Untargeted metabolomics analysis of liver chips

Collect the effluent (microfluid) from the liver chip. Following the standard tissue sample processing method, analyze the samples using LC-MS technology. For a comprehensive description of the data analysis methodology, please consult the Supplementary materials.

2.7. Molecular docking experimental procedure

First, conduct a molecular qualitative analysis of the aqueous extract of osmanthus to identify six substances: flavonoids, terpenoids, organic acids, phenolic acids, lipids, and glycerophospholipids. From each category, select the top three substances with the highest content, as presented in Table S1. For a detailed description of the experimental procedures and methods for molecular docking, please refer to the Supplementary materials.

2.8. Confocal imaging and quantitative morphometric analysis

A laser scanning confocal microscope was employed to acquire fluorescence images of the organ chips, with excitation filters set to 488 nm, 635 nm, and 405 nm, respectively. Quantitative fluorescence analysis was conducted using ImageJ.

2.9. Statistical analysis

The statistical analysis and graphing of the data results were carried out using GraphPad Prism 9.5 software. All measurements were performed in five replicates and are presented as mean ± standard deviation (SD). One-way analysis of variance (ANOVA) was employed to determine the statistical differences among groups. The least significant difference (LSD) method was used to compare the differences between each dose group and the Control group. Compared with the Control group, *: $p < 0.05$, **: $p < 0.01$; compared with the DBP 50 μM group, #: $p < 0.05$, ##: $p < 0.01$; compared with the DBP 50 μM + VitC group, Δ: $p < 0.05$, ΔΔ: $p < 0.01$; compared with the t-BHP group, &: $p < 0.05$, &&: $p < 0.01$; compared with the t-BHP + VitC group, δ: $p < 0.05$, δδ: $p < 0.01$; ns: $p > 0.05$. (Note: When the highly significant difference was either $p < 0.01$ or $p < 0.001$, it was uniformly represented by $p < 0.01$).

3. Results

3.1. OSF alleviates DBP/t-BHP-induced liver organoid injury through the Nrf2/PPAR-α pathway

As shown in Fig. 3B, the oxidative stress results from liver organoids illustrate the effects of different treatments on in vivo oxidative stress status, revealing varying outcomes across treatment groups. The Control group established a baseline with relatively stable oxidative stress indicators, providing fundamental reference values. In the DBP 50 μM group, markers indicative of DNA oxidative damage (8-OHdG) and lipid peroxidation (MDA) were significantly elevated, while pro-inflammatory cytokines (TNF-α, IL-6, IL-1β) exhibited varying degrees of upregulation. This indicates that DBP induced pronounced oxidative stress and inflammatory responses, a pattern similarly observed in the t-BHP group. The combination of different OSF concentrations with DBP demonstrated beneficial antagonistic effects, with higher OSF concentrations exhibiting stronger suppression of DBP-induced oxidative stress. This suggests that OSF enhances cellular resistance to DBP-induced oxidative damage by activating the Nrf2 pathway and upregulating downstream antioxidant enzymes (e.g., HO-1). The VitC group, as a classical antioxidant, efficiently regulated multiple key oxidative stress indicators. When DBP 50 μM combined with OSF 200 μM was administered alongside t-BHP, oxidative stress damage was significantly

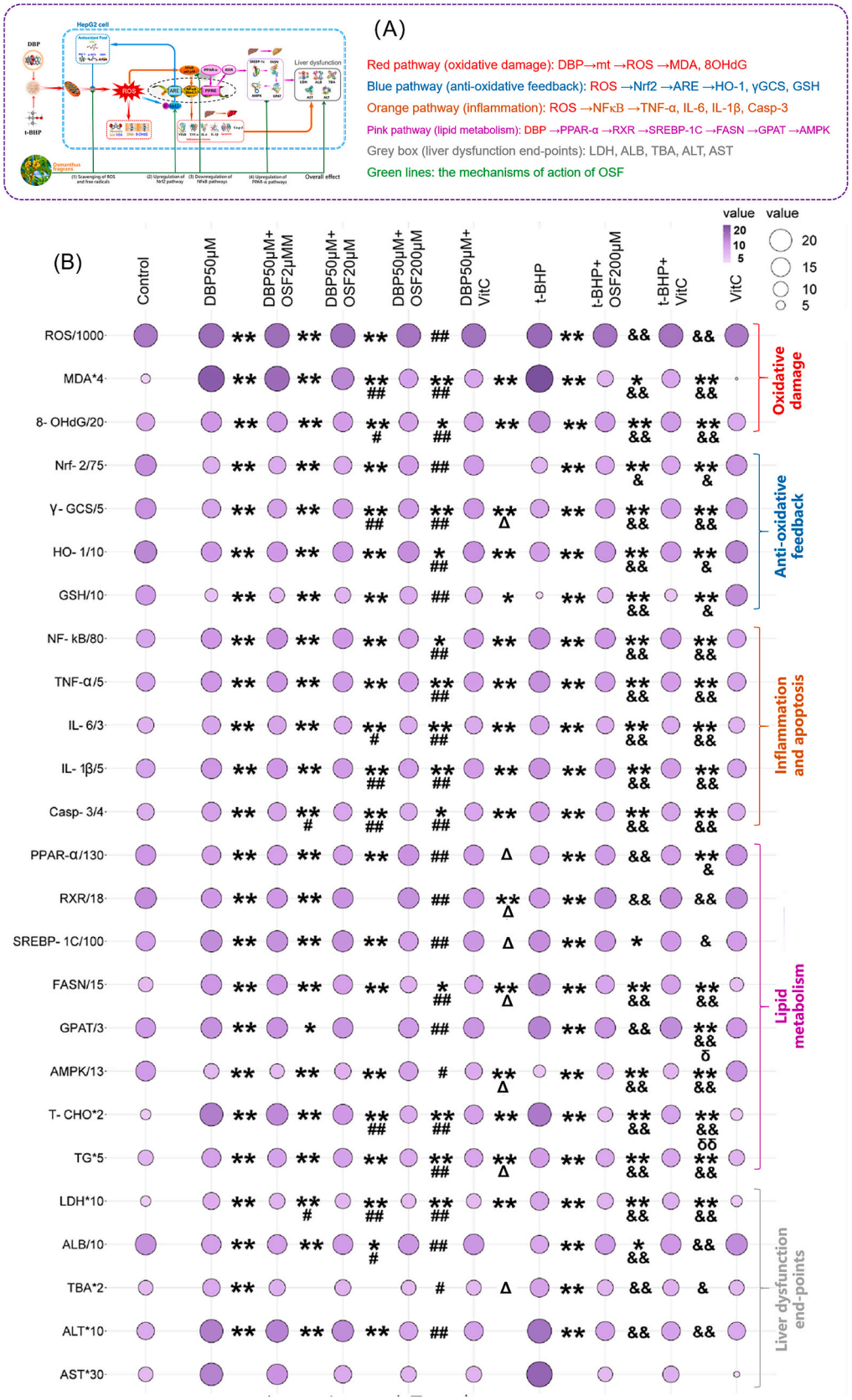

Fig. 3. Molecular Pharmacological Test Results of Liver Organoids. (A) Six different mechanisms in this study; (B) Analysis of specific index results under five different pathways. ($n = 5$, compared with the control group, *: $p < 0.05$, **: $p < 0.01$; compared with the DBP 50 μM group, #: $p < 0.05$, ##: $p < 0.01$; compared with the DBP 50 μM + VitC group, Δ: $p < 0.05$, ΔΔ: $p < 0.01$; compared with the t-BHP group, &: $p < 0.05$, &&: $p < 0.01$.)

reduced to levels comparable with VitC, indirectly suggesting that the antioxidative potential of OSF may rival that of VitC.

Fig. 3B presents the results of lipid metabolism in liver organoids. In the Control group, all lipid metabolism indicators consistently maintained normal expression levels. In the DBP 50 μM group, the expression of PPAR-α and RXR was significantly downregulated, leading to impaired lipid catabolism. Conversely, factors promoting lipid synthesis, such as SREBP-1c and FASN, exhibited a marked increase in activity, accelerating triglyceride synthesis. Detection results indicated substantially elevated levels of T-CHO and TG, disrupting lipid metabolic homeostasis. The t-BHP group also displayed disorders in lipid metabolism, characterized by inhibited AMPK activity (the cellular energy sensor), which further disturbed the lipid metabolism signaling pathway. The groups treated with varying concentrations of OSF in combination with DBP showed positive changes: OSF was able to upregulate the expression of PPAR-α. Although the changes were subtle at lower concentrations, a mitigating trend was already evident. At medium concentrations, the expression of PPAR-α and RXR demonstrated some recovery, while the activity of lipid synthesis-related factors slightly decreased. The most significant changes were observed in the DBP 50 μM + OSF 200 μM group, where PPAR-α and RXR levels nearly normalized, lipid synthesis factors were suppressed, and T-CHO and TG levels significantly declined. This suggests that high concentrations of OSF can effectively counteract DBP-induced lipid metabolism disorders. Additionally, when VitC was used in combination with DBP and t-BHP, it also contributed to bringing key lipid metabolism indicators closer to the levels observed in the Control group, underscoring the significant potential of OSF in regulating lipid metabolism.

The results of liver function in liver organoids are shown in Fig. 3B. In the Control group, all indicators remained stable, with values within the healthy range, indicating that liver metabolic and detoxification functions were operating effectively. In the DBP 50 μM group, the levels of AST, ALT, and LDH increased significantly, suggesting liver cell damage, altered membrane permeability, and the release of numerous intracellular enzymes into the bloodstream. Concurrently, the content of TBA also increased, indicating a blockage in bile excretion or synthesis processes, which significantly disturbed liver function. A similar pattern was observed in the t-BHP group, where several enzyme indicators exhibited abnormal fluctuations, implying oxidative stress damage to the liver and a subsequent decline in liver function. When various concentrations of OSF were combined with DBP, a tendency for alleviation was noted even at low concentrations, with more pronounced effects at medium and high concentrations. The levels of AST, ALT, and LDH gradually decreased and approached those of the Control group, suggesting that OSF can mitigate the hepatotoxicity induced by DBP. As a positive control, the VitC group effectively regulated the enzyme indicators and improved liver function. Notably, when high-concentration OSF was combined with t-BHP, the liver function-related indicators returned to the normal range to varying degrees, demonstrating the potential of OSF in protecting liver function.

3.2. *Immunofluorescence staining reveals the protective effect of OSF against DBP-and t-BHP-induced liver organoid injury*

Throughout the research process, the conclusions were supported by ALB, ZO-1, and nucleus-specific staining, while potential interferences were excluded through the strict execution of operational procedures. The experimental results were not influenced by the physical size of the microspheres. Although the physical size of VitC microspheres was larger than that of other groups, rigorous verification confirmed that this factor did not significantly interfere with the experimental results, thereby ensuring the accuracy and reliability of the data (Leary et al., 2016; Sae-be et al., 2022). Notably, an overlap of ZO-1 staining with the nucleus was observed, indicating its association with perinuclear organelles near protein synthesis sites (Chang et al., 2017).

The results are presented in Fig. 4. The liver organoid staining experiment clearly illustrates the differences among each group. In the Control group, the staining of ZO-1, ALB, and the nucleus exhibited normal cell architecture and protein expression. In the DBP 50 μM group, the fluorescence intensity of ALB was significantly reduced, and

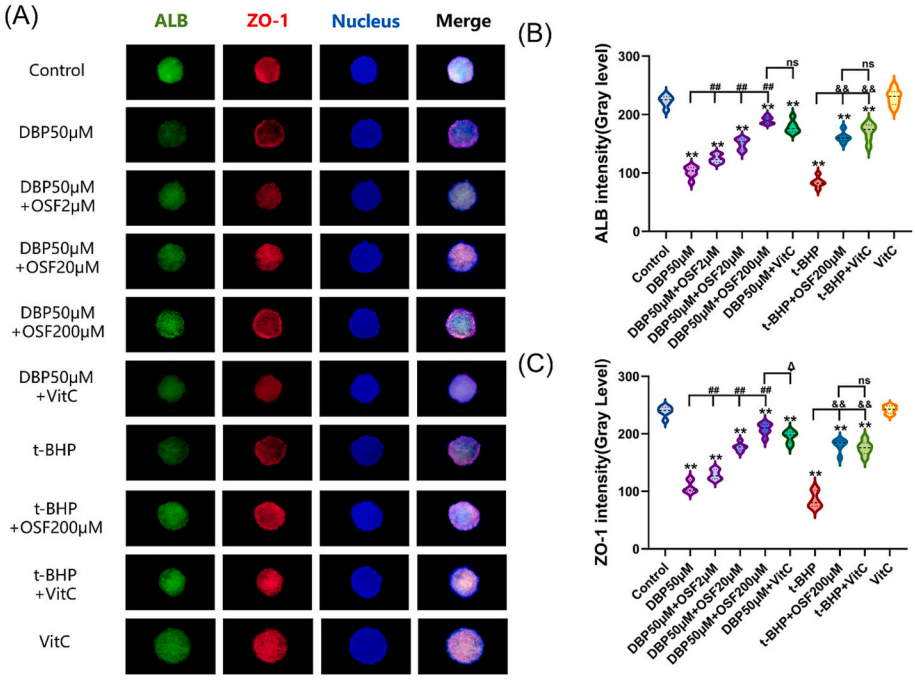

Fig. 4. Immunofluorescence Staining Results of Liver Organoids. (A) Represent the immunofluorescence staining images of liver organoids, where red indicates ZO-1, green represents ALB, and blue denotes cell nucleus; (B) Represent the fluorescence Quantification Level of Albumin; (C) Represent the fluorescence Quantification Level of Tight-Junction Proteins. ($n = 6$, compared with the control group, **: $p < 0.01$; Compared with the DBP 50 μM group, ##: $p < 0.01$; Compared with the DBP 50 μM + VitC group, Δ: $p < 0.05$; Compared with the t-BHP group, &&: $p < 0.01$; ns: $p > 0.05$.) (For interpretation of the references to colour in this figure legend, the reader is referred to the web version of this article.)

its distribution range was narrowed, indicating that liver synthetic function was inhibited. The fluorescence of ZO-1 appeared blurred or even absent, suggesting damage to the tight junctions between cells and impairment of the organoids' structural integrity. Additionally, the morphology of the nuclei displayed irregular changes, with some nuclei either shrinking or swelling, indicating an abnormal cellular state. The situation was more severe in the t-BHP group, where the staining results reflected significant damage to the tissue structure. Conversely, in the groups protected by OSF, as the concentration of DBP 50 μM increased, ZO-1 gradually became clearer and more continuous, the expression of ALB steadily recovered, and the nuclear morphology returned to normal, demonstrating a significant protective effect. The staining in the VitC group was normal, underscoring its antioxidant and stabilizing effects. Furthermore, the groups with high-concentration OSF combined with t-BHP, as well as those with VitC combined with both types of damaging agents, exhibited varying degrees of tissue repair, providing a viable approach for alleviating liver injury.

3.3. Immunofluorescence staining analysis of liver organ chips: Damage effects of DBP and t-BHP and protective role of OSF

In this study, immunofluorescence staining analysis was carried out using HepG2 3D liver organ chips (Fig. 5), the results of immunofluorescence staining of the liver organ chips reveal significant differences among the various experimental groups. In the Control group, ZO-1 delineates clear and complete cell boundaries, ALB is evenly distributed, and the nuclei exhibit a regular shape, indicating a normal physiological state. In the DBP 50 μM group, the continuity of ZO-1 deteriorates, presenting multiple breaks, while the fluorescence of ALB diminishes, suggesting an inhibition of synthetic function. Additionally, the nuclei appear deformed and shrunken, reflecting the detrimental impact of this substance. The situation is exacerbated in the t-BHP group, where the tissue structure is severely compromised. In the three groups combining OSF with DBP 50 μM, an increase in concentration correlates with a gradual recovery of ZO-1 coherence, intensified ALB fluorescence, and a trend towards regularity in nuclear shape, indicating a progressive emergence of protective effects. The staining in the VitC group is entirely normal. Furthermore, groups with high-concentration OSF combined with t-BHP, as well as those with VitC combined with DBP 50 μM and t-BHP, also demonstrate varying degrees of improvement, offering hope for the repair of liver injury.

3.4. Metabolomics analysis reveals the impact of OSF on the metabolic profile of liver tissue exposed to DBP

With the advancement of omics research, metabolomics analysis has gradually become a crucial method for exploring the impact of external factors on the metabolism of organisms or organs. To further investigate the molecular mechanisms underlying the repair effects of OSF on liver injury, we performed metabolomic profiling and analysis of the microfluidic effluents from liver chips models under two conditions: DBP 50 μM and DBP 50 μM + OSF 200 μM. Principal component analysis (PCA) revealed significant differences between the metabolic profiles of the two groups (Fig. 6A). The identified metabolites were primarily categorized as lipids and lipid-like molecules, organic acids and derivatives, organoheterocyclic compounds, and organic oxygen compounds (Fig. 6B). Differential metabolites were screened based on VIP values from OPLS-DA analysis, fold change, and *p*-values from univariate analysis, and a volcano plot of the differential metabolites was generated (Fig. 6C). A total of 558 significantly different metabolites were identified between the two groups. Classification of these differential metabolites showed that phospholipids, aminoglycosides, and carboxylic acids were the dominant compound categories (Fig. 6D). To visualize the trend of changes in differential metabolites between the groups and

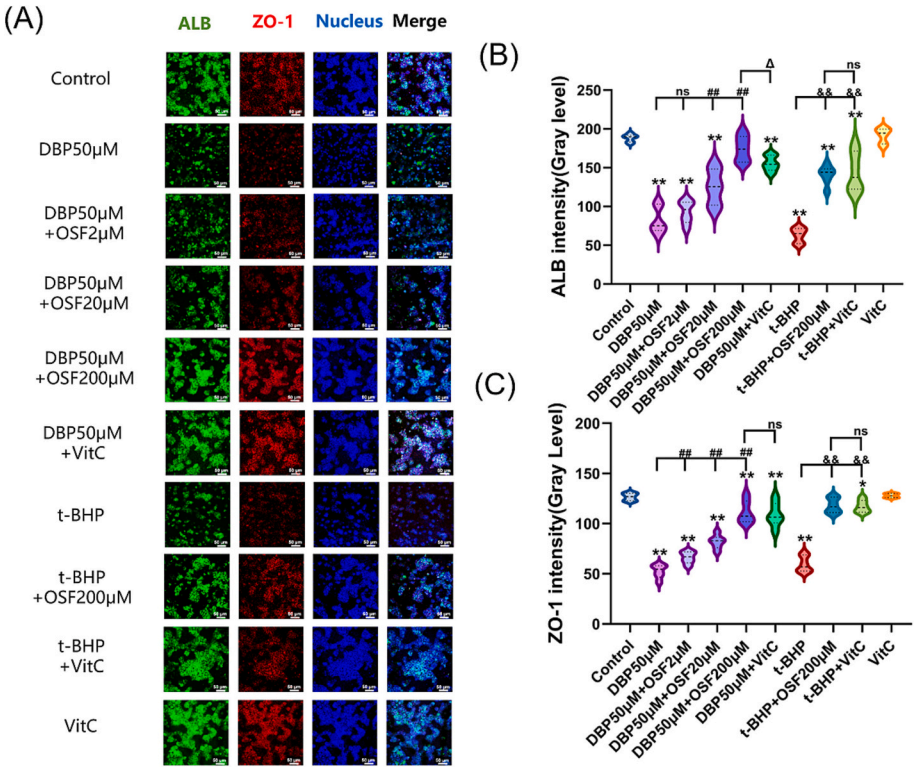

Fig. 5. Immunofluorescence staining images of HepG2 liver organ chips. (A) Represent the immunofluorescence staining images of organ chips; (B) Represent the fluorescence Quantification Level of ALB; (C) Represent the fluorescence Quantification Level of ZO-1. (n = 6, compared with the control group, *: $p < 0.05$, **: $p < 0.01$; Compared with the DBP 50 μM group, ##: $p < 0.01$; Compared with the DBP 50 μM + VitC group, Δ: $p < 0.05$; Compared with the t-BHP group, &&: $p < 0.01$; ns: $p > 0.05$.)

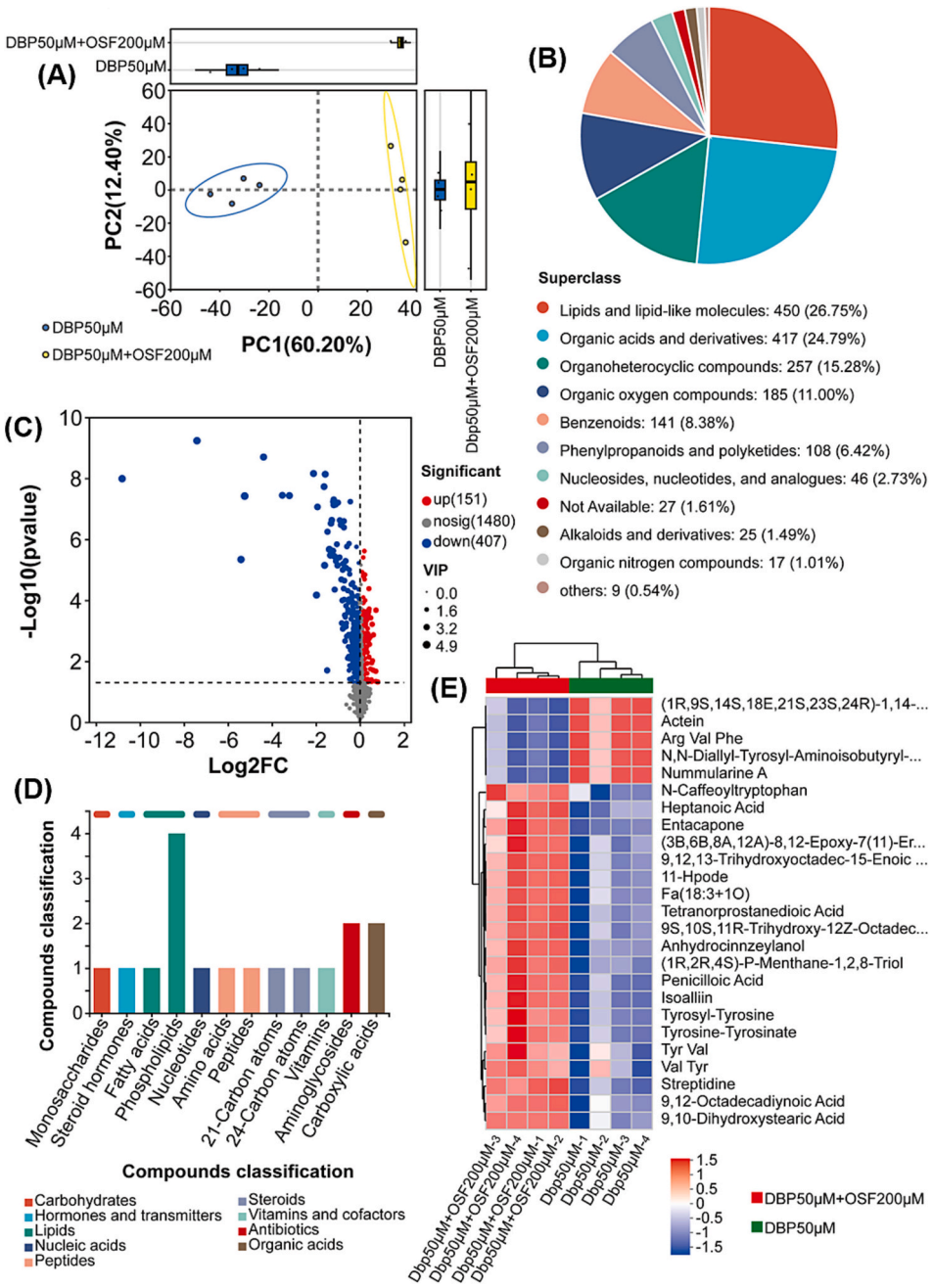

Fig. 6. Effects of OSF on the metabolic profiles of the microfluidic effluents in the liver organ chips. (A) PCA analysis; (B) Classification of detected compounds in samples; (C) Volcano plot of differential metabolites between DBP 50 μM and DBP 50 μM + OSF 200 μM; (D) Classification of differential metabolites; (E) Heatmap of cluster analysis of differential metabolites.

identify significantly upregulated or downregulated metabolites, clustering analysis was performed (Fig. 6E), and the top 25 significantly different metabolites were listed. In metabolomic analysis, these differential metabolites are often mapped to KEGG pathways to identify significantly enriched metabolic pathways, which aids in better understanding the potential molecular mechanisms suggested by these metabolites (Fig. 7A). Enrichment analysis identified significantly altered metabolic pathways (*t*-test, $p < 0.05$), including: Linoleic acid metabolism; Alanine, aspartate, and glutamate metabolism; Systemic lupus erythematosus; Pathogenic *Escherichia coli* infection; Autophagy-other; Glycerophospholipid metabolism; Drug metabolism-cytochrome P450; Primary bile acid biosynthesis; Tryptophan metabolism; and Glycosylphosphatidylinositol-anchor biosynthesis. Compared to the DBP 50 μM group, the pathways significantly upregulated in the DBP 50 μM + OSF 200 μM group included: Systemic lupus erythematosus; Pathogenic *Escherichia coli* infection; Autophagy-other; Glycerophospholipid metabolism; and Primary bile acid biosynthesis. The pathways significantly downregulated included: Linoleic acid metabolism; Alanine, aspartate, and glutamate metabolism; Drug metabolism-cytochrome P450; and Tryptophan metabolism (Fig. 7B).

3.5. *Molecular docking analysis reveals the binding mechanism between active components of OSF and liver injury repair target proteins*

The interaction between the active molecular ligands of osmanthus flowers and the target proteins is evaluated according to the binding energy scores. The higher the score, the greater the possibility that the ligand binds to the relevant target protein. In the molecular simulation,

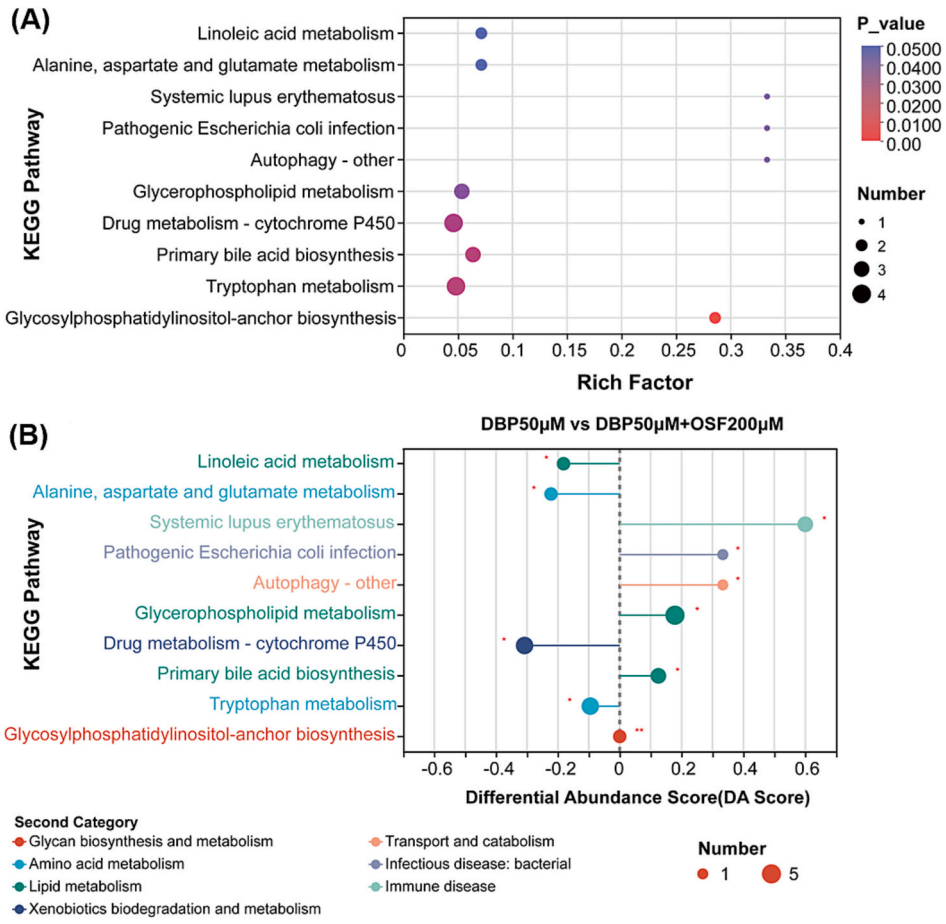

Fig. 7. KEGG enrichment analysis of differential metabolites. (A) Bubble plot of KEGG enrichment analysis; (B) Plot of differential abundance scores in KEGG pathways.

six selected active ingredients in the OSF and four protein targets were considered, as shown in Table S2. Firstly, regarding the interaction between the six types of compounds and the Nrf2 target protein, the flavonoid compound MeHesp has the highest binding energy (−9.119) in its interaction with Nrf2; for the interaction between the six types of compounds and the PPAR-α target protein, the glycerophospholipid compound PE has the highest binding energy (−9.481) in its interaction with PPAR-α; for the interaction between the six types of compounds and the FASN target protein, the glycerophospholipid compound PE has the highest binding energy (−9.674) in its interaction with FASN; for the interaction between the six types of compounds and the RXR target protein, the flavonoid compound Isorhamnetin has the highest binding energy (−8.765) in its interaction with RXR. Secondly, among the interactions between the four proteins and the flavonoid compounds, the interaction between MeHesp and Nrf-2 has the highest binding energy (−9.119); among the interactions between the four proteins and the terpenoid compounds, the interaction between Lig and Nrf-2 has the highest binding energy (−8.885); among the interactions between the four proteins and the organic acid compounds, the interaction between 3S-5-(1R,2S,3R,4aR,8aR)-3,4-DHP-acid and Nrf-2 has the highest binding energy (−8.351); among the interactions between the four proteins and the phenolic acid compounds, the interaction between Fos and Nrf-2 has the highest binding energy (−8.767); among the interactions between the four proteins and the lipid compounds, the interaction between (9*S*,10*S*)-9-POA-10-OH and RXR has the highest binding energy (−8.746); among the interactions between the four proteins and the glycerophospholipid compounds, the interaction between PE and FASN has the highest binding energy (−9.674). As shown in Fig. 8, we finally selected the 8 most representative pairs of molecular docking complexes mentioned above (Nrf-2-MeHesp Complex, Nrf-2-Fos Complex, Nrf-2-Lig Complex, Nrf-2-3S-5-(1R,2S,3R,4aR,8aR)-3,4-DHP-acid Complex, RXR-I3ORha (1–2)βGal Camplex, RXR-3S-5-(1R,2S,3R,4aR,8aR)-3,4-DHP Complex, FASN-PE Complex, PPARα-PE Complex) for result display. These compound-target interactions show good binding affinities to the proteins, which confirms the protein-ligand interactions in the network.

4. Discussions

This study integrated liver organoids, liver organ chips models, and the HepG2 cell line to deeply explore the interaction between OSF and DBP at the levels of oxidative stress and hepatic lipid metabolism, providing a multi-dimensional perspective and abundant data support for liver-related research. As advanced in vitro liver research models, liver organoids and liver organ chips are more accurate in replicating the complex tissue structure of the liver and the network of intercellular interactions compared with traditional monolayer cell cultures. This not only helps to gain a deeper understanding of the physiological processes of the liver but also provides a more reliable platform for studying the impact of exogenous substances on the liver. The HepG2 cell line, as a typical liver cell model among them, has many similarities in its biological characteristics and liver functions and is a commonly used tool for studying liver metabolism, toxic reactions, and so on.

This study confirms that the common environmental pollutant DBP exhibits significant toxicity to liver organ chip, liver organoids, and HepG2 cells. At the level of oxidative stress, DBP increases intracellular levels of ROS, MDA, and 8-OHdG, disrupts redox homeostasis, and triggers lipid peroxidation of cell membranes (elevated MDA) and DNA

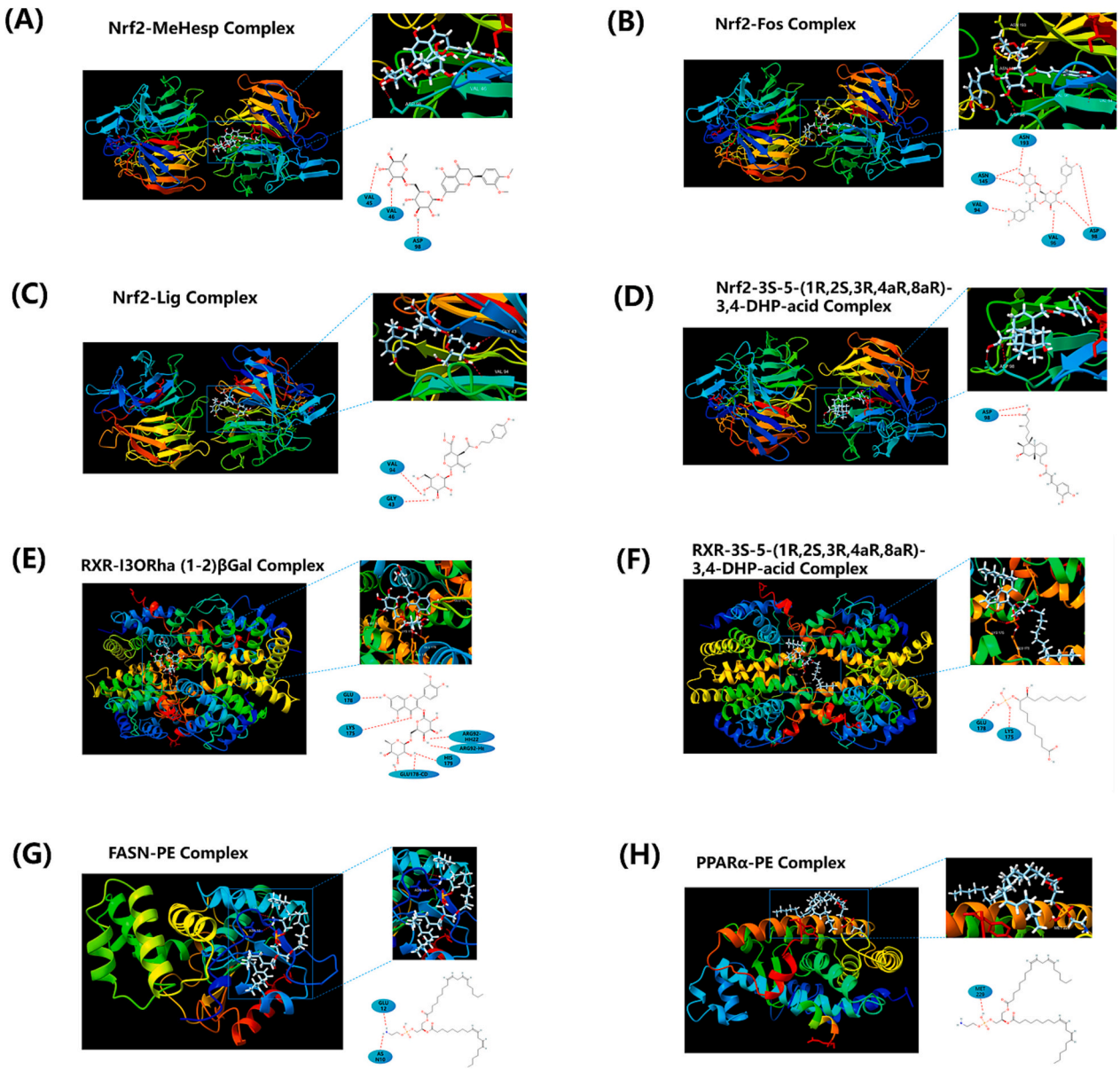

Fig. 8. Display of eight representative complexes in molecular docking. (A) Nrf2-MeHesp Complex; (B) Nrf2-Fos Complex; (C) Nrf2-Lig Complex; (D) Nrf2-3S-5-(1R,2S,3R,4aR,8aR)-3,4-DHP-acid Complex; (E) RXR-I3ORha (1–2)β-Gal Complex; (F) RXR-3S-5-(1R,2S,3R,4aR,8aR)-3,4-DHP Complex; (G) FASN-PE Complex; (H) PPAR-α-PE Complex.

oxidation (increased 8-OHdG) through ROS chain reactions, thereby impairing cellular function. At the level of lipid metabolism, DBP downregulates the expression of PPAR-α and AMPK, while upregulating the expression of SREBP-1c and GPAT, leading to the accumulation of T-CHO and TG. This interferes with the hepatic metabolic regulatory network by inhibiting fatty acid oxidation and promoting lipid synthesis. Conversely, OSF exhibits protective effects against DBP-induced injury: it dose-dependently reduces ROS, MDA, and 8-OHdG levels under oxidative stress, potentially by activating the Nrf-2 signaling pathway (upregulating γ-GCS and HO-1) to enhance endogenous antioxidant capacity. In lipid metabolism, OSF reverses DBP-induced T-CHO and TG accumulation by restoring PPAR-α and AMPK expression while inhibiting SREBP-1c and GPAT. These findings indicate that OSF can restore lipid metabolic homeostasis and alleviate DBP-induced hepatic steatosis and metabolic disorders through precise regulation of metabolic signaling molecules and enzyme activities.

Metabolomics analysis indicates that OSF can alleviate DBP-induced liver injury by regulating metabolites and remodeling metabolic pathways. Twenty-five significantly different metabolites, including 9,10-dihydroxystearic acid and 9,12-octadecadienoic acid, are involved in lipid metabolism, oxidative stress, and signal transduction regulation. The enhancement of unsaturated fatty acid metabolism improves cell membrane fluidity, while the upregulation of the glycerophospholipid metabolic pathway corroborates this effect. Additionally, the decreased abundance of metabolites such as Nummularine A suggests that OSF can inhibit the generation of oxidative damage molecules. In amino acid metabolism, the regulation of metabolites such as Val and Tyr, along with the metabolic pathways of alanine/aspartate/glutamate and tryptophan, can alleviate metabolic disorders caused by oxidative stress and promote cell repair. The downregulation of the linoleic acid metabolic pathway reduces oxidative stress damage, while the upregulation of the primary bile acid synthesis pathway enhances the liver's detoxification function. Furthermore, the downregulation of the cytochrome P450 drug metabolism pathway inhibits the generation of toxic intermediates. Cluster analysis reveals that upregulated metabolites, such as 11-Hpode, are associated with antioxidant protection, while downregulated

metabolites, such as Actein, serve as pathological metabolic markers; their reduced abundance confirms the inhibitory effect of OSF. In summary, OSF restores metabolic homeostasis to repair liver function through multi-target regulation of lipid and amino acid metabolism, as well as oxidative stress pathways.

Molecular docking technology holds an extremely important position in fields such as drug development and biochemistry research. It can predict the interaction patterns and binding affinities between small molecules and target proteins, providing strong evidence for in-depth understanding of biomolecular mechanisms and the screening of potentially active molecules. The results of molecular docking have revealed the unique interaction patterns of each complex. As shown in Table S2 and Fig. 8, in (A) the Nrf-2-MeHesp Complex, (B) the Nrf-2-Fos Complex, and (C) the Nrf-2-Lig Complex, Nrf-2 binds to different ligands, providing clues for exploring its transcriptional regulation mechanisms and helping to understand the cell's antioxidant stress response. (D) The Nrf-2-3S-5-(1R,2S,3R,4aR,8aR)-3,4-DHP-acid Complex has expanded the boundaries of Nrf-2-related research. Meanwhile, (E) the RXR-I3ORha (1–2) βGal Complex and (F) the RXR-3S-5-(1R,2S,3R,4aR,8aR)-3,4-DHP Complex focus on RXR, contributing to the interpretation of nuclear receptor functions. (G) The FASN-PE Complex and (H) the PPAR-α-PE Complex are associated with key enzymes and receptors in lipid metabolism, which are of great significance for the research on lipid metabolism disorders.

This study has two limitations. First, the absence of an OSF (200 μM) group has resulted in insufficient comparative dimensions. Future independent experiments will utilize Western blotting and proteomics to compare the molecular mechanisms and dose-response relationships between VitC and OSF. Second, the sample size did not meet expectations, leading to inadequate statistical power. The non-targeted metabolomics analysis was limited to two groups, excluding control and DBP + VitC groups, among others. Additional groups will be incorporated in future experiments to enhance the reliability of the conclusions. Future analyses will combine Western Blot and Q-PCR to quantitatively assess the expression of related proteins, thereby minimizing bias associated with a single method.

5. Conclusions

In conclusion, this study not only revealed the harmful mechanism of DBP on the liver model systems but also highlighted the potential application value of OSF in combating such hazards. However, the exact molecular targets and signal transduction networks through which OSF exerts its effects still need to be further analyzed in depth, and translational research from in vitro models to in vivo practical applications also needs to be carried out, with the expectation of providing a more solid theoretical basis and practical guidance for the development of liver protection strategies based on natural products.

Supplementary data to this article can be found online at https://doi.org/10.1016/j.foodres.2025.116976.

CRediT authorship contribution statement

Qing Feng: Writing – review & editing, Writing – original draft, Visualization, Software, Resources, Methodology, Formal analysis, Data curation, Conceptualization. **Hongguo Chen:** Writing – review & editing, Writing – original draft, Visualization, Software, Methodology, Data curation, Conceptualization. **Meng Ren:** Writing – review & editing, Writing – original draft. **Yongkang Qiao:** Writing – review & editing, Writing – original draft, Visualization, Software, Resources, Conceptualization. **Jingjing Zou:** Writing – review & editing, Writing – original draft, Data curation. **Xiao Liang:** Writing – review & editing, Writing – original draft, Software. **Ling Yu:** Writing – review & editing, Writing – original draft. **Yang Wu:** Writing – review & editing, Writing – original draft. **Shaohui Chen:** Writing – review & editing, Writing – original draft. **Yanling Sun:** Writing – review & editing, Writing – original draft. **Cuiyu Bao:** Writing – review & editing, Validation. **Xu Yang:** Writing – review & editing, Writing – original draft, Visualization, Validation, Software, Resources, Project administration, Methodology. **Ping Ma:** Writing – review & editing, Validation, Resources, Project administration, Investigation, Funding acquisition, Conceptualization. **Surui Lu:** Writing – review & editing, Writing – original draft, Visualization, Software, Methodology, Data curation, Conceptualization.

Declaration of competing interest

The authors declare that they have no known competing financial interests or personal relationships that could have appeared to influence the work reported in this paper.

Acknowledgments

This study was supported by the National Natural Science Foundation of China (42177416), Key Special Project for Social Development R&D of Xianning City Science and Technology Program (2023SFYF095), and Scientific Research Innovative Team of Hubei University of Science and Technology (2023T08).

Data availability

Data will be made available on request.

References

Ahammed, B., & Kalangi, S. K. (2024). A decade of organoid research: Progress and challenges in the field of organoid technology. *ACS Omega, 9*(28), 30087–30096. https://doi.org/10.1021/acsomega.4c03683

Banerjee, P., Gaddam, N., Chandler, V., & Chakraborty, S. (2023). Oxidative stress-induced liver damage and Remodeling of the liver vasculature. *The American Journal of Pathology, 193*(10), 1400–1414. https://doi.org/10.1016/j.ajpath.2023.06.002

Brooks, A., Liang, X., Zhang, Y., Zhao, C. X., Roberts, M. S., Wang, H., … Crawford, D. H. G. (2021). Liver organoid as a 3D in vitro model for drug validation and toxicity assessment. *Pharmacological Research, 169*, Article 105608. https://doi.org/10.1016/j.phrs.2021.105608

Chang, C. H., Yen, M. C., Liao, S. H., Hsu, Y. L., Lai, C. S., Chang, K. P., & Hsu, Y. L. (2017). Secreted protein acidic and rich in cysteine (SPARC) enhances cell proliferation, migration, and epithelial mesenchymal transition, and SPARC expression is associated with tumor grade in head and neck cancer. *International Journal of Molecular Sciences, 18*(7), 1556. https://doi.org/10.3390/ijms18071556

Cheng, L., Li, J., Cheng, J., & Wu, Z. (2019). DBP-induced activation of ROS and ERK1/2 causes hepatic and renal damage in Kunming mice. *Human & Experimental Toxicology, 38*(8), 938–950. https://doi.org/10.1177/0960327119843583

Deng, S., Li, C., Cao, J., Cui, Z., Du, J., Fu, Z., Yang, H., & Chen, P. (2023). Organ-on-a-chip meets artificial intelligence in drug evaluation. *Theranostics, 13*(13), 4526–4558. https://doi.org/10.7150/thno.87266

El-Kenawi, A., & Ruffell, B. (2017). Inflammation, ROS, and mutagenesis. *Cancer Cell, 32*(6), 727–729. https://doi.org/10.1016/j.ccell.2017.11.015

Farooqi, H. M. U., Kang, B., Khalid, M. A. U., Salih, A. R. C., Hyun, K., Park, S. H., … Choi, K. H. (2021). Real-time monitoring of liver fibrosis through embedded sensors in a microphysiological system. *Nano Convergence, 8*(1), 3. https://doi.org/10.1186/s40580-021-00253-y

Fu, C. C., Xu, F. Y., Qian, Y. C., Koo, H. L., Duan, Y. F., Weng, G. M., … Zhu, F. Y. (2022). Secondary metabolites of *Osmanthus fragrans*: Metabolism and medicinal value. *Frontiers in Pharmacology, 13*, Article 922204. https://doi.org/10.3389/fphar.2022.922204

Hernández-Mesa, M., Le Bizec, B., & Dervilly, G. (2021). Metabolomics in chemical risk analysis - A review. Analytica Chimica Acta, 1154 (0), 338298. Doi: https://doi.org/10.1016/j.aca.2021.338298.

Huang, B., Zhao, M., Yang, M., Rao, L., Wu, C., Hu, Y., … Li, Y. (2022). *Osmanthus fragrans* loaded NIPAAM hydrogel promotes osteogenic differentiation of MC3T3-E1. *Gels, 8*(10), 659. https://doi.org/10.3390/gels8100659

Huang, H. B., Cheng, P. K., Siao, C. Y., Lo, Y. C., Chou, W. C., & Huang, P. C. (2022). Mediation effects of thyroid function in the associations between phthalate exposure and lipid metabolism in adults. *Environmental Health: A Global Access Science Source, 21*(1), 61. https://doi.org/10.1186/s12940-022-00873-9

Huang, S. K., Bueno, P. R. P., Garcia, P. J. B., De Lee, M. J., Castro-Cruz, K. A., Leron, R. B., & Tsai, P. W. (2023). Antioxidant, anti-inflammatory and antiproliferative effects of *Osmanthus fragrans* (Thunb). Lour. flower extracts. *Plants (Basel, Switzerland), 12*(17), 3168. https://doi.org/10.3390/plants12173168

Kanabekova, P., Kadyrova, A., & Kulsharova, G. (2022). Microfluidic organ-on-a-chip devices for liver disease modeling in vitro. *Micromachines, 13*(3), 428. https://doi.org/10.3390/mi13030428

Leary, E., Rhee, C., Wilks, B., & Morgan, J. R. (2016). Accurate quantitative wide-field fluorescence microscopy of 3-D spheroids. *Biotechniques, 61*(5), 237–247. https://doi.org/10.2144/000114472

Liu, X., & Locasale, J. W. (2017). Metabolomics: A primer. *Trends in Biochemical Sciences, 42*(4), 274–284. https://doi.org/10.1016/j.tibs.2017.01.004

Long, S., Dong, X., Tan, B., Zhang, S., Xie, S., Chi, S., Liu, H., Deng, J., Yang, Y., & Zhang, H. (2021). Growth performance, antioxidant ability, biochemical index in serum, liver histology and hepatic metabolomics analysis of juvenile hybrid grouper (♀ *Epinephelus fuscoguttatus* × ♂ *Epinephelus lanceolatus*) fed with oxidized fish oil. *Aquaculture, 545*. https://doi.org/10.1016/j.aquaculture.2021.737261, 737261-737261.

Luo, L. Y., Xue, R., Wang, T. G., Zhang, J. W., Li, S., Li, J. C., … Zhang, Y. Z. (2024). The ethanolic extract of *Osmanthus fragrans* var. thunbergii flowers ameliorates depressive-like behaviors of mice by modulating the serotonin system and suppressing neuroinflammation. *Food Science & Nutrition, 12*(9), 6242–6258. https://doi.org/10.1002/fsn3.4270

Mastrangeli, M., & van den Eijnden-van Raaij, J. (2021). Organs-on-chip: The way forward. *Stem Cell Reports, 16*(9), 2037–2043. https://doi.org/10.1016/j.stemcr.2021.06.015

Miao, L., Zhang, J., Yin, L., & Pu, Y. (2022). Metabolomics analysis reveals alterations in cochlear metabolic profiling in mice with noise-induced hearing loss. *BioMed Research International, 2022*, 9548316. https://doi.org/10.1155/2022/954831

Moradi, E., Jalili-Firoozinezhad, S., & Solati-Hashjin, M. (2020). Microfluidic organ-on-a-chip models of human liver tissue. *Acta Biomaterialia, 116*, 67–83. https://doi.org/10.1016/j.actbio.2020.08.041

Murphy, M. P. (2009). How mitochondria produce reactive oxygen species. *The Biochemical Journal, 417*(1), 1–13. https://doi.org/10.1042/BJ20081386

Murthy, S. S., & Narsaiah, T. B. (2021). Cytotoxic effect of bromelain on HepG2 hepatocellular carcinoma cell line. *Applied Biochemistry and Biotechnology, 193*(6), 1873–1897. https://doi.org/10.1007/s12010-021-03505-z

Panwar, A., Das, P., & Tan, L. P. (2021). 3D hepatic organoid-based advancements in LIVER tissue engineering. *Bioengineering (Basel, Switzerland), 8*(11), 185. https://doi.org/10.3390/bioengineering8110185

Pingitore, P., Sasidharan, K., Ekstrand, M., Prill, S., Lindén, D., & Romeo, S. (2019). Human multilineage 3D spheroids as a model of liver steatosis and fibrosis. *International Journal of Molecular Sciences, 20*(7), 1629. https://doi.org/10.3390/ijms20071629

Ribeiro, A. J. S., Yang, X., Patel, V., Madabushi, R., & Strauss, D. G. (2019). Liver microphysiological systems for predicting and evaluating drug effects. *Clinical Pharmacology and Therapeutics, 106*(1), 139–147. https://doi.org/10.1002/cpt.1458

Sae-be, A., Wiwatpanit, T., Varatthan, T., Namporn, T., Laungkulldej, S., Thiabma, R., … Ruenraroengsak, P. (2022). Comparative study between the 3D-liver spheroid models developed from HepG2 and immortalized hepatocyte-like cells with primary hepatic stellate coculture for drug metabolism analysis and anticancer drug screening. *Advanced Therapeutics, 6*(2), 237–247. https://doi.org/10.2144/000114472

Septiana, W. L., Noviantari, A., & Antarianto, R. D. (2023). Induced pluripotent stem cells (Ipscs) based liver organoid: The benefits and challenges. *Cellular Physiology and Biochemistry, 57*(5), 345–359. https://doi.org/10.33594/000000662

Sun, W., Chen, Y., Luo, G., Zhang, M., Zhang, H., Wang, Y., & Hu, P. (2016). Organs-on-chips and its applications. *Chinese Journal of Analytical Chemistry, 44*(4), 533–541. https://doi.org/10.1016/s1872-2040(16)60920-9

Wang, Y., Gao, Y., Pan, Y., Zhou, D., Liu, Y., Yin, Y., Yang, J., Wang, Y., & Song, Y. (2023). Emerging trends in organ-on-a-chip systems for drug screening. *Acta Pharmaceutica Sinica B, 13*(6), 2483–2509. https://doi.org/10.1016/j.apsb.2023.02.006

Wu, L., Guo, T., Deng, R., Liu, L., & Yu, Y. (2021). Apigenin ameliorates insulin resistance and lipid accumulation by endoplasmic reticulum stress and SREBP-1c/SREBP-2 pathway in palmitate-induced HepG2 cells and high-fat diet-fed mice. *The Journal of Pharmacology and Experimental Therapeutics, 377*(1), 146–156. https://doi.org/10.1124/jpet.120.000162

Yang, S., Hu, H., Kung, H., Zou, R., Dai, Y., Hu, Y., Wang, T., Lv, T., Yu, J., & Li, F. (2023). Organoids: The current status and biomedical applications. *MedComm, 4*(3), Article e274. https://doi.org/10.1002/mco2.274

Zhang, C., Zhang, K., Chai, Z., Song, Y., Wang, X., Duan, Y., & Zhang, M. (2022). Identification of miRNAs and target genes at key stages of sexual differentiation in androdioecious *Osmanthus fragrans*. *International Journal of Molecular Sciences, 23*(18), 10386. https://doi.org/10.3390/ijms231810386

Zheng, R., Liu, C., Wang, Y., Luo, J., Zeng, X., Ding, H., … Wang, C. (2017). Expression of MEP pathway genes and non-volatile sequestration are associated with circadian rhythm of dominant terpenoids emission in *Osmanthus fragrans* lour. flowers. *Frontiers in Plant Science, 8*, 1869. https://doi.org/10.3389/fpls.2017.01869

Zhu, M., Du, X., Xu, H., Yang, S., Wang, C., Zhu, Y., … Zhao, W. (2021). Metabolic profiling of liver and faeces in mice infected with echinococcosis. *Parasites & Vectors, 14*(1), 324. https://doi.org/10.1186/s13071-021-04807-1